1 **TITLE:**

2 ***In vivo* KRAS G12D/V Degradation Mediated by CANDDY Using a Modified**

3 **Proteasome Inhibitor**

4

5 **AUTHORS/AFFILIATIONS:**

6 **Satoshi Imanishi[1,#], Lijuan Huang[1,#], Shoko Itakura[2], Masamichi Ishizaka[1],**

7 **Megumi Tsukamoto[1], Megumi Saito[1], Yoichi Iwasaki[1], Tomohiro Yamaguchi[1], and**

8 **Etsuko Miyamoto-Sato[1,2*]**

9 [1] Laboratory of Miyamoto-Sato Molecular Medical Sciences, Research Institute for

10 Science & Technology, Tokyo University of Science, 2641 Yamazaki, Noda, Chiba

11 278-0022, Japan

12 [2]Graduate School of Biological Sciences, Tokyo University of Science, 2641 Yamazaki,

13 Noda, Chiba 278-0022, Japan

14

15 [#]These authors contributed equally to this work.

16 [*] Correspondence: nekoneko@rs.tus.ac.jp

Summary paragraph

"Undruggable" proteins, such as RAS proteins, remain problematic despite efforts to discover inhibitors against them. KRAS mutants are prevalent in human cancers. Although KRAS G12C inhibitors have been developed recently, there are no effective inhibitors for KRAS G12D/V. Here, we described the development of a novel chemical knockdown strategy, termed CANDDY (Chemical knockdown with Affinity aNd Degradation DYnamics). This strategy, which is not an inhibition strategy, involves a CANDDY tag modified from a proteasome inhibitor. The tag induces direct proteasomal degradation. We constructed TUS-007 as a multispecific small molecule tethered from a KRAS interactor and CANDDY tag to target KRAS G12D/V. TUS-007 successfully suppressed tumors due to the degradation of KRAS G12D/V. We confirmed that the CANDDY tag-induced degradation was independent of target ubiquitination. The CANDDY technology could represent a simple and practical way to degrade currently "undruggable" proteins.

31 The majority (75%) of disease-causing proteins are "undruggable" (i.e., difficult to
32 inhibit with small molecules). This difficulty reflects in the presence of smooth surfaces
33 and lack of deep pockets, including proteins associated with cancer drivers and many
34 interfaces for protein-protein interaction (PPI) (1, 2, 3). RAS family members (e.g.,
35 KRAS, HRAS, and NRAS) are most challenging to inhibit by small molecules (1, 4, 5,
36 6, 7). Mutations of KRAS, especially G12C, G12D, and G12V, are frequent in human
37 cancers (7). The RAS protein activities depend on nucleotide loading in their GTP-
38 binding pockets. The inhibition of this pocket has been attempted for nearly 40 years.
39 However, progress has been hindered by the exceptionally high affinity between GTP
40 and RAS proteins (1, 4, 8). While clinically effective inhibitor candidates targeting
41 KRAS G12C have been developed recently (6, 9), there is still no effective inhibitor for
42 KRAS G12D/V. These are important targets found in 95% of pancreatic cancers and
43 64% of colon cancers (7, 8). Inhibitors of the PPI between RAS and Son of Sevenless 1
44 (SOS1) (RAS-SOS inhibitor) have been investigated. Inhibitors that directly bind to
45 RAS are not effective owing to their low affinity (5). Thus, the current inhibition
46 technologies are not enough to be effective for undruggable proteins.

47 Pharmaceutical research on undruggable proteins, such as RAS, focuses on novel
48 modalities instead of inhibition (10, 11, 12). Protein destabilization technologies, using
49 matchmakers between the target and E3 ligase for target ubiquitination, are expected to
50 be effective against undruggable proteins (13, 14, 15, 16, 17). However, matchmaker
51 design has been hampered by the dependency on target ubiquitination (16). It is difficult
52 to select a suitable E3 ligase for a target of interest because of limited knowledge about
53 the mechanism underlying substrate recognition by E3 ligases. Even if the target has an
54 established corresponding E3 ligase, there may be no available ligand for the E3 ligase.
55 Moreover, target ubiquitination may not always induce proteolysis, as in the case of
56 RAS, in which ubiquitination also regulates protein localization and activation (18).
57 Despite such difficulties, an effective inhibitor (9) was used recently for a proteolysis
58 inducer of KRAS G12C (19). However, no proteolysis inducer for KRAS G12D/V has
59 been reported. Current protein destabilization technologies that depend on
60 ubiquitination have limited efficacy for undruggable targets (14). Therefore, to
61 modulate diverse undruggable targets, the difficulties in matchmaking should be
62 eliminated (13).

63 Here, we report successful KRAS G12D/V degradation, mediated by a novel tool

64 named CANDDY (Chemical knockdown with Affinity aNd Degradation DYnamics).

65 This innovative approach induces direct proteasomal degradation (i.e., chemical

66 knockdown) of the target using a CANDDY tag derived from a proteasome inhibitor

67 that lacks the site for inhibitory activity (inhibitor site). In principle, chemical

68 knockdown occurs without ubiquitination, so it can bypass the difficulties of designing

69 a matchmaker in current protein destabilization techniques (13). To evaluate the utility

70 of CANDDY, we developed a CANDDY molecule called TUS-007 for KRAS G12D/V

71 and demonstrated its application in KRAS G12D/V chemical knockdown in cell-free, *in*

72 *vitro*, and *in vivo* assays and *in vivo* tumor suppression.

73

74 **A CANDDY molecule for targeting KRAS G12D/V proteins**

75 CANDDY molecules are bispecific molecules constructed from two modules;

76 a target interactor, which enables specific binding to the target, and a CANDDY tag,

77 which induces proteasomal degradation (Fig. 1a). The CANDDY tag is essential in

78 CANDDY technology and is a derivative lacking the inhibitor site of MLN2238 (MLN)

79 (20), a clinical proteasome inhibitor (Fig. 1b and Additional Information). To design

80 TUS-007, we employed a RAS-SOS inhibitor (5) (shown in Fig. 1c) which directly

81 binds to KRAS G12D, KRAS G12V, and wild-types of KRAS and HRAS as the target

82 interactor module. Since the binding to wild-type NRAS have not been reported, it was

83 expected to avoid the severe toxicity observed in a pan-RAS inhibitor (21). RAS-SOS

84 inhibitor was conjugated to the CANDDY tag using an NH_2 linker (Fig. 1c and

85 Additional Information).

86 To compare the target binding of TUS-007 with that of the RAS-SOS

87 inhibitor, we performed a thermal shift assay. Unexpectedly, KRAS G12D/V proteins

88 incubated with TUS-007 were more resistant against heat treatment than those

89 incubated with RAS-SOS inhibitor (Fig. 1d). Alternatively, in a fluorescence-based

90 thermal shift assay, the T_m value of KRAS G12D incubated with TUS-007 was higher

91 than that of KRAS G12D incubated with RAS-SOS inhibitor (Supplementary Fig. 1).

92 These results suggest the higher affinity of TUS-007 to KRAS compared to RAS-SOS

93 inhibitor. In addition, we confirmed that TUS-007 had no inhibitory activity against the

94 catalytic β-subunits of proteasome (Supplementary Fig. 2). This demonstrated that the

95 CANDDY tag, modified from a proteasome inhibitor, hardly inhibit proteasome

96 activity.

97

98 **A CANDDY molecule degraded KRAS G12D/V proteins in cell-free assay**

99 We attempted a chemical knockdown of KRAS G12D in the presence of 26S

100 proteasomes and in the absence of E3 ligase in a cell-free assay. Successful degradation

101 was performed (Fig. 1e) with 50% degradation concentration (DC50) at 4 μM

102 (Supplementary Fig. 3a). The chemical knockdown mediated by TUS-007 was

103 counteracted by the presence of MLN (Supplementary Fig. 3b). Additionally, RAS-

104 SOS-NH_2 as a degradation-incompetent control failed to induce the chemical

105 knockdown (Supplementary Fig. 3b), demonstrating CANDDY tag is essential to

106 induce the chemical knockdown. Although RAS-SOS inhibitor showed 80% inhibition

107 of RAS-SOS PPI at 1 mM (5), DC80 of TUS-007 for KRAS G12D was estimated as 16

108 μM (Supplementary Fig. 3a). It implied that the conjugation with CANDDY tag

109 drastically improved the usefulness of RAS-SOS inhibitor. We also confirmed chemical

110 knockdown of KRAS G12V by TUS-007 in a cell free assay (Supplementary Fig. 3c).

111 Thus, the chemical knockdown of KRAS G12D/V by TUS-007 depended only on

112 proteasomes and not on ubiquitination. Importantly, the conjugation of CANDDY tag

113 enabled the direct proteasomal induction and the simple cell free assay for chemical

114 knockdown could be applied, because of the lack of ubiquitination process.

115

116 **TUS-007 induced targets-selective chemical knockdown *in vitro***

117 Using an *in vitro* assay, we then evaluated the chemical knockdown and

118 investigated the selectivity of TUS-007. We utilized RAS-less mouse embryonic

119 fibroblasts (MEFs) expressing human KRAS G12D, G12V, or G12C. These MEFs do

120 not proliferate in the absence of RAS (22). Immunoblotting analysis revealed that TUS-

121 007 induced the chemical knockdown of KRAS G12D/V, but not G12C, in RAS-less

122 MEFs (Fig. 1f). TUS-007 reduced the viability of RAS-less MEFs expressing KRAS

123 G12D/V but did not affect the viability of the cells expressing KRAS G12C (Fig. 1g),

124 confirming the selectivity of TUS-007 for KRAS G12D/V. Moreover, the results from

125 RAS-less MEFs expressing KRAS G12C showed that TUS-007 did not cause non-

126 specific cytotoxic effects even for high concentrations such as 100 μM (Fig. 1f & g).

127 Additionally, we assessed the selectivity of TUS-007 for the human RAS family,

128 including wild-type KRAS, HRAS, and NRAS. TUS-007 did not affect the NRAS

129 protein levels or the viability of RAS-less MEFs expressing NRAS but attenuated

130 KRAS and HRAS levels and reduced the viability of RAS-less MEFs expressing KRAS

131 and HRAS (Supplementary Fig. 4a and b). This result is consistent with the previously

132 reported data on the selectivity of the RAS-SOS inhibitor (5). Therefore, considering

133 that TUS-007 is not a pan-RAS degrader, it is expected not to induce intolerable

134 toxicity, as has been previously observed with a pan-RAS inhibitor *in vivo* (21).

135 Furthermore, the viability of RAS-less MEFs expressing KRAS G12C or NRAS

136 maintained even at 100 μM TUS-007. These results suggested that TUS-007 did not

137 have remarkable off-target effect resulting in toxicity in cell even at high

138 concentrations.

139

140 **TUS-007 exerted anti-tumor activity against KRAS G12V-driven colon cancer**

141 Approximately 64% of human colon cancers reportedly express KRAS

142 mutants. KRAS G12V is found in nearly half of the patients and is correlated with poor

143 prognosis (8). Therefore, we investigated whether TUS-007 can suppress the growth of
144 human KRAS G12V-driven colon cancer cells. We conducted an experiment with the
145 SW620-Luc KRAS G12V homozygous human colon cancer cell line (23). TUS-007
146 induced chemical knockdown of KRAS (Fig. 2a), accompanied by an increase in the
147 annexin V-positive fraction in SW620-Luc cells (Fig. 2b). However, RAS-SOS-NH_2 (a
148 synthetic intermediate without CANDDY tag, Fig. 1c) and cetuximab did not induce
149 apoptosis (Fig. 2b and Supplementary Fig. 5). In contrast, treatment with TUS-007 did
150 not result in significant changes in the annexin V-positive fraction in HT29-Luc RAS-
151 independent colon cancer cells (Fig. 2c and Supplementary Fig. 6). Alternatively, the
152 apoptosis induction in SW620-Luc cells was confirmed by caspase 3/7 activation (Fig.
153 2d). Importantly, TUS-007 induced the apoptosis in SW620-Luc cells at the same
154 concentration at which the chemical knockdown of KRAS was significant (Fig. 2a and
155 b). These findings indicated that TUS-007 selectively induces apoptosis in SW620-Luc
156 cells by chemical knockdown of KRAS G12V *in vitro*. Additionally, the results in
157 HT29-luc cells also indicated no remarkable off-target effect resulting in toxicity even
158 at high concentrations.

159 Next, to assess the effectiveness of TUS-007 *in vivo*, we transplanted SW620-
160 Luc cells subcutaneously in immunodeficient mice. TUS-007 or cetuximab was
161 administered to the xenograft mice by intraperitoneal (i.p.) injection. TUS-007
162 significantly attenuated tumor progression (Fig. 2e; Supplementary Fig. 7a and b) and
163 induced KRAS G12V chemical knockdown in tumors (Fig. 2f). The body weights of
164 the mice were not affected by TUS-007 treatment (Supplementary Fig. 7c). These
165 results suggested that TUS-007 is effective *in vivo* against KRAS G12V-driven tumors.
166

167 **TUS-007 exerted anti-tumor activity against KRAS G12D-driven pancreatic**
168 **cancer**

169 Approximately 95% of pancreatic cancers harbor KRAS mutations, and the
170 G12D mutation is particularly prevalent and strongly correlated with poor prognosis (8).
171 Therefore, we examined the effects of TUS-007 in human pancreatic cancer cell lines.
172 As expected, TUS-007 degraded the KRAS protein (Fig. 3a) and induced apoptosis
173 (Fig. 3b) in SW1990 KRAS G12D-driven pancreatic cancer cells (24). In addition,
174 apoptosis was induced with caspase 3/7 activation in SW1990 cells (Fig. 3c), which was

175 counteracted by the proteasome inhibitor MLN but not by the NAE E3 ligase inhibitor

176 (NAEi) (Fig. 3d). Furethermore, the apoptosis induction in SW1990 cells was detected

177 around concentrations of chemical knockdown of KRAS (Fig. 3a and b). Therefore, it

178 suggested that TUS-007 induced apoptosis owing to target degradation independent of

179 ubiquitination.

180 In mice with SW1990 cells implanted subcutaneously, the oral (per os; p.o.)

181 administration of TUS-007 significantly suppressed the tumor growth (Fig. 3e and

182 Supplementary Fig. 8a) and reduced tumor weight (Supplementary Fig. 8b). The i.p.

183 injection of TUS-007 also supressed subcutaneously implanted tumor growth in mice

184 (Supplementary Fig. 8c). Both p.o. (Fig. 3f) and i.p. (Supplementary Fig. 8d)

185 administrations showed no change in body weight. Here, we examined the chemical

186 knockdown of KRAS, HRAS and NRAS with TUS-007 in pancreas from the identical

187 mice used in Fig. 3e & f. In accordant with the results in RAS-less MEFs, TUS-007

188 induced the degradation of KRAS and HRAS but not NRAS (Supplementary Fig 10).

189 Thus, there was no sign of toxicity such as body weight losses in contrast to a pan-RAS

190 inhibitor (21).

191 Moreover, extracellular signal-regulate kinase (ERK) and AKT

192 phosphorylation were decreased by both p.o. and i.p. administrations (Supplementary

193 Fig. 9a & b), indicating that both RAS-mitogen-activation protein (RAS-MAP) and

194 RAS- phosphoinositide 3-kinase (RAS-PI3K) signaling were inhibited. It is difficult for

195 inhibitors to inhibit both RAS-MAP and RAS-PI3K signaling, even using a clinically

196 effective KRAS G12C inhibitor (6). Thus, the chemical knockdown of KRAS by

197 CANDDY might offer a clinical benefit. Taken together, these results indicated that

198 TUS-007 exerted *in vivo* antitumor activity *via* the chemical knockdown of KRAS

199 G12D/V and suppression of KRAS signaling.

200 Here, when an i.p dose of 80 mg/kg TUS-007 was administered to healthy

201 mice, a concentration (45 ng/mg, equivalent to 53 μM) of TUS-007 was observed in the

202 pancreas (Supplementary Table 1.). This TUS-007 concentration *in vivo* agreed with the

203 concentration at which chemical knockdown and apoptotic indicators were observed in

204 SW1990 cells *in vitro* (Fig. 3a, b and c). Therefore, these results suggest that there is no

205 contradiction between our *in vivo* and *in vitro* results.

206

207 **TUS-007 exerted anti-tumor activity even in orthotopic xenograft model mice**

208 Finally, SW1990-Luc cells were transplanted directly into the pancreas of
209 mice as an orthotopic xenograft model. The mice were subsequently treated p.o. with
210 TUS-007. Remarkably, *in vivo* imaging revealed reductions in tumor growth (Fig. 4a
211 and b; Supplementary Fig. 11a) and tumor weight (Supplementary Fig. 11b). Results
212 from immunohistochemical analysis (Fig. 4c left panels and left bar graph) and
213 immunoblotting (Supplementary Fig. 11c) confirmed the chemical knockdown of
214 KRAS G12D in the tumor tissues of mice treated with TUS-007. Furthermore, higher
215 concentrations of positive cells were observed in the terminal deoxynucleotidyl
216 transferase dUTP nick-end labeling (TUNEL) assay in the tumor tissues of TUS-007-
217 treated mice, implying the induction of apoptosis in the TUS-007-treated tumors (Fig.
218 4c right panels and right bar graph). The body weights of the orthotopic xenograft
219 model mice were not affected by TUS-007 (Supplementary Fig. 11d). Overall, these
220 results demonstrated that oral treatment with TUS-007 induces KRAS G12D chemical
221 knockdown and suppresses pancreatic tumor growth without the sign of weight loss and
222 significant toxicity in the orthotopic xenograft model.

223

224 **CANDDY applied to another undruggable target**

225 To evaluate the versatility of CANDDY approach, we designed a CANDDY

226 molecule targeting MDM2 (MDM2-CANDDY), a negative regulator of P53, using a

227 P53-MDM2 PPI inhibitor (25) as an interactor module of a CANDDY molecule

228 (Supplementary Fig. 12a and Additional Information). MDM2-CANDDY successfully

229 induced the chemical knockdown of MDM2 in HCT-116 human colon cancer cells

230 (Supplementary Fig. 12b). Although the reactivation of P53 by inhibition of MDM2 has

231 been expected as a novel therapeutic approach (26), P53-MDM2 PPI is still well-

232 recognized "undruggable" target. This result suggested the potential versatility of

233 CANDDY to target other undruggable proteins.

234

235 No effective drug to inhibit or degrade KRAS G12D/V has been reported yet.

236 TUS-007 successfully induced chemical knockdown of KRAS G12D/V, resulting in

237 tumor suppression *in vivo*. Generally, it has been difficult to find effective inhibitors for

238 undruggable targets. Nevertheless, just conjugating CANDDY tag to RAS-SOS

239 inhibitor produced TUS-007, an effective agent even for oral administrations *in vivo*.

240 Our results demonstrated that TUS-007 induced chemical knockdown of KRAS

241 G12D/V *via* a proteasomal process, which was independent of ubiquitination.

242 Importantly, we confirmed that chemical knockdown of KRAS induced

243 apoptosis (Fig. 2a and b; Fig. 3a and b). Also, the consistency between our *in vivo* and

244 *in vitro* results was confirmed by the pancreatic concentration of TUS-007, which

245 agreed with the effective concentratin *in vitro* (Fig. 3a, b and c; Supplementary Table1).

246 Additionally, a previous study showed that the moderate decrease of KRAS

247 protein inhibited tumor growth via more strong inhibition of downstream signal (12),

248 similarly as that in Supplementary Fig. 9a & b. In fact, the chemical knockdown of

249 KRAS by TUS-007 was moderate (Supplementary Fig. 11c) but suppressed the tumor

250 growth *in vivo* (Fig. 4a and b). The future study of TUS-007 may overcome the current

251 clinical challenge related to the treatment refractory nature of KRAS G12D/V-positive

252 neoplasms.

253 The CANDDY tag, which was modified from a proteasome inhibitor, can

254 eliminate the difficulties of matchmaking in current protein degradation (13),

255 considering that proteasomes, unlike E3 ligases, have no substrate selectivity.

256 Moreover, CANDDY tag was also effective in degrading MDM2 (Supplementary Fig.

257 12). These results suggest that CANDDY technology could be applied to other

258 undruggable targets without efficient inhibitors. Hence, CANDDY technology could

259 provide a simple and practical approach to induce the chemical knockdown of currently

260 undruggable targets.

261

262 **References**

263 1. Khan, I., Rhett, J. M. & O'Bryan, J. P. Therapeutic targeting of RAS: New Hope for

264 drugging the "undruggable". *Biochim. Biophys. Acta Mol. Cell Res.* **1867**, 118570

265 (2020).

266 2. Fujimori, S., et al. Next-generation sequencing coupled with a cell-free display

267 technology for high-throughput production of reliable interactome data. *Sci. Rep.* **2,**

268 691 (2012).

269 3. Scott, D. E., Bayly, A. R., Abell, C. & Skidmore, J. Small molecules, big targets:

270 Drug discovery faces the protein-protein interaction challenge. *Nat. Rev. Drug*

271 *Discov.* **15,** 533–550 (2016).

272 4. Stephen, A. G., Esposito, D., Bagni, R. K. & McCormick, F. Dragging Ras back in

273 the ring. *Cancer Cell* **25,** 272–281 (2014).

274 5. Sun, Q., et al. Discovery of small molecules that bind to K-Ras and inhibit Sos-

275 mediated activation. *Angew. Chem. Int. Ed.* **51,** 6140–6143 (2012).

276 6. Canon, J., et al. The clinical KRAS(G12C) inhibitor AMG 510 drives anti-tumour

277 immunity. *Nature* **575,** 217–223 (2019).

278 7. Hobbs, G. A., Der, C. J. & Rossman, K. L. RAS isoforms and mutations in cancer at
279 a glance. *J. Cell Sci.* **129,** 1287–1292 (2016).
280 8. Haigis, K. M. KRAS alleles: The devil is in the detail. *Trends Cancer* **3,** 686–697
281 (2017).
282 9. Sheridan, C. Grail of RAS cancer drugs within reach. *Nat. Biotechnol.* **38,** 6–8
283 (2020).
284 10. Shin, S. M., et al. Antibody targeting intracellular oncogenic Ras mutants exerts
285 anti-tumour effects after systemic administration. *Nat. Commun.* **8,** 15090 (2017).
286 11. Yin, W. & Rogge, M. Targeting RNA: A transformative therapeutic strategy. *Clin.*
287 *Transl. Sci.* **12,** 98–112 (2019).
288 12. Ross, S. J., et al. Targeting KRAS-dependent tumors with AZD4785, a high-affinity
289 therapeutic antisense oligonucleotide inhibitor of KRAS. *Sci. Transl. Med.* **9,** pii:
290 eaal5253. doi: 10.1126/scitranslmed.aal5253 (2017).
291 13. Deshaies, R. J. Multispecific drugs herald a new era of biopharmaceutical
292 innovation. *Nature* **580,** 329–338 (2020).

293 14. Scudellari, M. Protein-slaying drugs could be the next blockbuster therapies. *Nature*
294 **567,** 298–300 (2019).
295 15. Cromm, P. M. & Crews, C. M. Targeted protein degradation: From chemical
296 biology to drug discovery. *Cell Chem. Biol.* **24,** 1181–1190 (2017).
297 16. Pettersson, M. & Crews, C. M. PROteolysis TArgeting Chimeras (PROTACs) -
298 Past, present and future. *Drug Discov. Today Technol.* **31,** 15–27 (2019).
299 17. Churcher, I. Protac-induced protein degradation in drug discovery: Breaking the
300 rules or just making new ones? *J. Med. Chem.* **61,** 444–452 (2018).
301 18. Dohlman, H. G. & Campbell, S. L. Regulation of large and small G proteins by
302 ubiquitination. *J. Biol. Chem.* **294,** 18613–18623 (2019).
303 19. Bond, M. J., et al. Targeted degradation of oncogenic KRASG12C by VHL-
304 recruiting PROTACs. *ACS Cent. Sci.* **6**, 1367–1375 (2020).
305 20. Kisselev, A. F., van der Linden, W. A. & Overkleeft, H. S. Proteasome inhibitors:
306 An expanding army attacking a unique target. *Chem. Biol.* **19,** 99–115 (2012).
307 21. Welsch, M. E., et al. Multivalent small-molecule pan-RAS inhibitors. *Cell* **168,**
308 878–889.e29 (2017).

309 22. Drosten, M., et al. Genetic analysis of Ras signaling pathways in cell proliferation,
310 migration and survival. *EMBO J.* **29,** 1091–1104 (2010).
311 23. Ahmed, D., et al. Epigenetic and genetic features of 24 colon cancer cell lines.
312 *Oncogenesis* **2,** e71 (2013).
313 24. Jansen, J. M., et al. Inhibition of prenylated KRAS in a lipid environment. *PLOS*
314 *ONE* **12,** e0174706 (2017).
315 25. Kumar, S. K., et al. Design, synthesis, and evaluation of novel boronic-Chalcone
316 derivatives as antitumor agents. *J. Med. Chem.* **46**, 2813–2815 (2003).
317 26. Shangary, S. & Wang, S. Targeting the MDM2-p53 Interaction for Cancer Therapy.
318 *Clin. Cancer. Res.* **14,** 5318–5324 (2008).
319

320 **Data availability**

321 Source data are provided for all experiments. Other data that support the

322 findings of this study are available from the corresponding author, upon reasonable

323 request.

324

325 **Acknowledgments** We thank Masaaki Ozawa, Mai Hasegawa, Takuya Yogi, Mizuki

326 Kanazawa, and Sachi Tsuji for help with the *in vitro* studies, Yuri Sato for help with the

327 *in vivo* studies. We thank the NCI RAS initiative for providing the RAS-less MEFs used

328 in this work, the Uchiro Laboratory for performing the high-resolution mass

329 spectrometry analysis at the Research Equipment Center (Tokyo University of Science

330 (TUS), Japan), the Gunji Laboratory (TUS) for the use of their high-performance liquid

331 chromatography instruments, the Iwakura and Abe Laboratories in the animal facility of

332 the Research Institute for Biomedical Sciences (TUS) for maintaining the mice, Fumito

333 Ishizuka and Naoki Takeda (NARD Institute, Ltd.) for contributions to the chemical

334 synthesis, and Hiroyuki Ohashi for the helpful suggestions. This work was financially

supported by the Program for Creating STart-ups from Advanced Research and Technology (START Program: 962238), and the joint research with FuturedMe Inc.

Author contributions S. Im., L. H., S. It., and E. M. S. designed the study. S. Im., L. H., S. It., M. I., M. T., M. S. and T. Y. performed the *in vitro* and *in vivo* experiments. Y. I. performed chemical analyses. E. M. S. supervised the study. All authors discussed the study and approved the submitted manuscript.

Competing interests The authors declare no competing interests.

Additional Information is available in the online version of the paper.

348 **Figure legends**

349

350 **Fig. 1. RAS chemical knockdown *in vitro*.**

351 **a,** Principle of the CANDDY technology. Each CANDDY molecule includes a target

352 interactor (burgundy hexagon) and a CANDDY tag (yellow oval). The target protein is

353 bound by the CANDDY molecule *via* the target interactor and is directly degraded by

354 proteasome via the CANDDY tag. **b,** The CANDDY tag was synthesized by chemically

355 inactivating the inhibitor site of MLM2238 (MLN). **c,** Structures of the RAS-SOS

356 inhibitor (ref. 3), RAS-SOS-NH_2, and TUS-007. **d,** Evaluation of the target-binding

357 affinity of TUS-007 to KRAS mutants by a thermal shift assay. Recombinant KRAS

358 was treated with the vehicle, RAS-SOS inhibitor, or TUS-007 for 30 min, heated at the

359 indicated temperature for 20 min, then analyzed by immunoblotting. **e,** KRAS G12D

360 protein level was lower after incubation with TUS-007 at the indicated concentrations in

361 the presence of 26S proteasome, indicating successful KRAS G12D degradation by

362 TUS-007 (mean ± SEM; n = 3). *$P < 0.05$ and ** $P < 0.01$ vs. DMSO. **f,** KRAS G12D

363 and G12V levels, but not the G12C level, were decreased in RAS-less MEFs after

364 incubation with TUS-007 for 72 h. Representative blots are shown. The relative

365 amounts of KRAS mutants normalized to GAPDH are shown in the bar graph (mean ±

366 SEM; n = 3–4). *P < 0.05 and ** P < 0.01 vs. DMSO. **g,** Decreased cell viability was

367 observed in RAS-less MEFs expressing human KRAS G12D and G12V, but not those

368 expressing G12C, after incubation with TUS-007 for 72 h (mean ± SEM; n = 3–4). *P <

369 0.05 and ** P < 0.01 vs. DMSO.

370

371

372 **Fig. 2. Chemical knockdown and tumor suppression *in vitro* and *in vivo* in KRAS**

373 **G12V-driven human colon cancer cells by TUS-007 treatment.**

374 **a,** Immunoblotting analysis of KRAS G12V chemical knockdown in SW620-Luc cells

375 treated with TUS-007 for 48 h at the indicated doses. The KRAS band intensity was

376 normalized to that of GAPDH (mean ± SEM; n = 3). *P < 0.05 and ** P < 0.01 vs.

377 DMSO. **b & c,** TUS-007 induced apoptosis in colon cancer SW620-Luc cells (b) but

378 not in HT29-Luc cells (c), a KRAS-independent, BRAF-dependent cell line (Ctx +

379 Vem: 100 mg/ml cetuximab and 40 μM vemurafenib). Cells were treated with each

380 compound for 48 h in terms of the number of annexin V-positive/PI-negative apoptotic

381 cells detected by flow cytometry (mean ± SEM; n = 2–5). **P < 0.01, and ***P < 0.001

382 vs. DMSO. **d,** Relative activity of caspase 3/7 in SW620-Luc cells treated with TUS-

383 007 or 5-fluorouracil (5-FU) for 48 h (mean ± SEM; n = 3). *P < 0.05 and ** P < 0.01

384 vs. DMSO. **e,** Tumor volume in mice with SW620-Luc cells transplanted

385 subcutaneously and treated with i.p. administration every 3 days (mean ± SEM; n = 6–

386 8). *P < 0.05 vs. vehicle alone. **f,** Immunoblotting of KRAS G12V chemical

387 knockdown in tumors from the same mice used in e (mean ± SEM; n = 6). **P < 0.01

388 vs. vehicle alone.

389

390 **Fig. 3. Chemical knockdown and tumor suppression *in vitro* and *in vivo* in KRAS**

391 **G12D-driven human pancreatic cancer cells by TUS-007 treatment.**

392 **a,** KRAS G12D chemical knockdown induced by TUS-007 in SW1990 cells. SW1990

393 cells were treated with TUS-007 for 72 h and analyzed by immunoblotting. The KRAS

394 G12D band intensity was normalized to that of GAPDH (mean ± SEM; n = 4). *P <

395 0.05 vs. DMSO. **b,** TUS-007 treatment for 72 h increased the proportion of annexin V-

396 positive apoptotic SW1990 cells compared with those treated with DMSO or RAS-

397 SOS-NH_2 (mean ± SEM; n = 3). *P < 0.05 vs. DMSO or RAS-SOS-NH_2. **c,** TUS-007

398 increased the caspase 3/7 activity in SW1990 cells after treatment for 96 h (mean ±

399 SEM; n = 3). *P < 0.05 and **P < 0.01 vs. DMSO. **d,** Caspase 3/7 activation by TUS-

400 007 was counteracted by proteasome inhibition by MLN2238 (MLN) but not by E3

401 ligase inhibition by NAE inhibitor in SW1990 cells treated with the agents for 96 h

402 (mean ± SEM; n = 3). **P < 0.01 vs. DMSO, ##P < 0.01 vs. TUS-007 (100 μM) only,

403 and †no statistically significant difference compared with TUS-007 (100 μM) only. **e,**

404 Tumor volume in mice with SW1990 cells transplanted subcutaneously and treated with

405 p.o. administered TUS-007 or vehicle (mean ± SEM; n = 6–9). The agents were

406 administered every 3 days. **P < 0.01 vs. vehicle alone. **f,** Body weight changes in

407 mice with SW1990 cells transplanted subcutaneously (mean ± SEM; n = 6–9). P.o.

408 treatment with TUS-007 did not affect the body weight.

409

410 **Fig. 4. TUS-007 suppresses the growth of KRAS G12D-positive orthotopic**

411 **pancreatic tumors.**

412 **a,** Images showing the luciferase activity and total flux in orthotopic tumors

413 transplanted SW1990-Luc cells *in vivo*. **b,** Tumor growth (bioluminescence) in identical

414 mice treated with vehicle or TUS-007 administered p.o. every 3 days. (mean ± SEM; n

415 = 6). *P < 0.05 vs. vehicle alone. **c,** Representative histochemical staining of KRAS and

416 TUNEL in orthotopic tumor sections from the same mice used in **a.** The scale bar is 60

417 μm. The bar graphs showed quantitative analyses of the KRAS G12D-positive area

418 (left) and TUNEL-positive area (right) (mean ± SEM; n = 6). **P < 0.01 vs. vehicle

419 alone.

420

421 **Supplementary Fig. 1. Estimation of T_m value of KRAS G12D incubated with TUS-**

422 **007.** KRAS G12D was mixed with DMSO, RAS-SOS inhibitor (4 μM) or TUS-007 (4

423 μM) and incubated under heating from 25 °C to 99 °C. The denature of KRAS G12D

424 was monitored by the fluorescence. The typical curve of each group was shown in upper

425 panels. The means of T_m values were shown in lower table (mean ± SEM; n = 2). * P <

426 0.05 vs. DMSO, # P < 0.05 vs. RAS-SOS inhibitor.

427

428 **Supplementary Fig. 2. Effects of TUS-007 on proteasome activity levels.**

429 The levels of chymotrypsin-like (b5), trypsin-like (b2), and caspase-like (b1)

430 proteasome activities was monitored by Suc-LLVY-AMC, Bz-VGR-AMC, and Z-LLE-

431 AMC, respectively. AMC fluorescence was monitored by a plate reader with excitation

432 and emission filters of 360 and 460 nm, respectively (DMSO, 30 min = 1) (mean ±

433 SEM; n = 2-3).

434

435 **Supplementary Fig. 3. TUS-007 induced degradation of KRAS G12D/V in cell free**

436 **assay.**

437 **a,** Evaluation of the correlation between relative amount of KRAS G12D and

438 concentration of TUS-007 were approximated with Rodbard. The DC50 was estimated

439 about 4 μM**. b,** A proteasome inhibitor MLN2238 repressed KRAS G12D chemical

440 knockdown by 26S proteasome. RAS-SOS inhibitor and RAS-SOS NH_2 did not induce

441 KRAS G12D chemical knockdown. KRAS G12D incubated with 26S proteasome and

442 agents as indicated for 3 h. **c,** KRAS G12V protein level was lower after incubation

443 with TUS-007 at the indicated concentrations in the presence of 26S proteasome for 1 h,

444 indicating successful KRAS G12V degradation by TUS-007 (mean ± SEM; n = 3). * P

445 < 0.05 vs. DMSO.

446

447 **Supplementary Fig. 4. Selective chemical knockdown of RAS variants in RAS-less**

448 **MEFs expressing different types of human RAS.**

449 **a,** Relative viability of RAS-less MEFs expressing WT human RAS family members

450 after incubation with TUS-007 or DMSO. (mean ± SEM; n = 3-5). *P < 0.05 and **P <

451 0.01 vs. DMSO. **b,** Degradation of WT human RAS family members in RAS-less MEFs

452 treated with TUS-007 or DMSO for 72 h (mean ± SEM; n = 4-5). *P < 0.05 and **P <

453 0.01 vs. DMSO.

454

455 **Supplementary Fig. 5. FACS plots for Annexin V- PI staining of SW620-Luc cells.**

456 SW620-Luc cells were treated with the indicated agents for 48 h, followed by staining

457 with Annexin V-FITC and PI. The typical plots are shown.

458

459 **Supplementary Fig. 6. FACS plots for Annexin V- PI staining of HT-29-Luc cells.**

460 HT-29-Luc cells were treated with the indicated agents for 48 h, followed by staining

461 with Annexin V-FITC and PI. The typical plots are shown.

462

463 **Supplementary Fig. 7. Effects of TUS-007 on the growth of colon cancer**

464 **subcutaneous xenografts and toxicity.**

465 **a,** Tumors of SW620-Luc cells at day 21 from the same mice shown in Fig. 2e (n = 6–

466 8). **b,** Comparison of SW620-Luc tumor weight at 21 days after injection (mean ± SEM;

467 n = 6–8). *P < 0.05 vs. vehicle alone. **c,** Body weight changes in mice with SW620-Luc

468 cells transplanted subcutaneously (mean ± SEM; n = 6–8). Treatment with TUS-007 did

469 not affect the body weight.

470

471 **Supplementary Fig. 8. Effects of TUS-007 on the growth of pancreatic cancer**

472 **subcutaneous xenografts and toxicity.**

473 **a,** Tumors of SW1990 cells from the same mice shown in Fig. 3e at 21 days after p.o.

474 administration. **b,** Comparison of SW1990 tumor weight in a in this figure at 21 days

475 after p.o. administration (mean ± SEM; n = 6-9). *P < 0.05 vs. vehicle alone. **c,** Tumor

476 volume in mice with SW1990 cells transplanted subcutaneously and treated with i.p.

477 administered TUS-007 or vehicle (mean ± SEM; n = 6-9). The agents were

478 administered every three days. *P < 0.05 vs. vehicle. **d,** Body weight changes in mice

479 with SW1990 cells transplanted subcutaneously (mean ± SEM; n = 6-9). i.p. treatment

480 with TUS-007 did not affect the body weight.

481

482 **Supplementary Fig. 9. Effect of TUS-007 on RAS signaling in of pancreatic cancer**

483 **subcutaneous xenografts.**

484 Immunoblotting of KRAS and downstream signaling molecules in tumors from the

485 same mice used in Fig 3a (**a**: p.o treatment) and Supplementary Fig.8c (**b**: i.p.

486 treatment). The quantitative analysis of the immunoblotting was shown as bar graph,

487 where the KRAS values were normalized to GAPDH, the p-ERK values were

488 normalized to the total ERK, and the p-AKT values were normalized to the total AKT

489 (mean ± SEM; n = 6). *P < 0.05 vs. vehicle.

490

491 **Supplementary Fig. 10. Effects of oral treatment with TUS-007 on wild type RAS**

492 **in pancreas.**

493 The immunoblotting analyses of wt RAS proteins in pancreas from the same mice

494 shown in Fig. 3e. TUS-007 degraded KRAS and HRAS but not NRAS (mean ± SEM; n

495 = 6-9). *P < 0.05 vs. vehicle alone.

496

497 **Supplementary Fig. 11. Effect of TUS-007 on growth of orthotopic pancreatic**

498 **cancer xenografts expressing mutant KRAS.**

499 **a,** Tumor growth, as assessed by luciferase signal, in individual mice orthotopically

500 transplanted SW1990-Luc cells treated with TUS-007 (red) or vehicle alone (blue)

501 (mean ± SEM; n = 6). **b,** Pancreases from orthotopic xenograft model mice at day 21

502 after treatment with TUS-007 (lower-left panel) or the vehicle alone (upper-left panel)

503 and comparison of their weights (right graph) (mean ± SEM; n = 6). *P < 0.05 vs.

504 vehicle alone. **c,** Immunoblotting of KRAS G12D in tumor lysates from the same mice

505 used in Fig. 4a. The bar graph shows quantification of KRAS G12D normalized to

506 GAPDH (mean ± SEM; n = 6). **P < 0.01 vs. vehicle alone. **d,** Body weight changes in

507 mice subjected to orthotopical transplantation of SW1990-Luc cells (mean ± SEM; n =

508 6). Treatment with TUS-007 did not affect the body weight.

509

510 **Supplementary Fig. 12. CANDDY induced degradation of MDM2, a common**

511 **undruggable target.**

512 **a,** The structure of MDM2-CANDDY using P53-MDM2 PPI inhibitor, with IC50 value

513 between 6-25 μM. **b,** The human colon cancer cells HCT-116 were incubated for 48 h

514 with MDM2-CANDDY. MDM2-CANDDY degraded MDM2 in the dose dependent

515 manner (mean ± SEM. n = 3). ** $P < 0.01$ vs. DMSO.

516

517

518 **Methods**

519

520 **Cell lines.** SW1990 and HCT-116 cells were purchased from the American Type

521 Culture Collection (Manassas, VA, USA). SW620-Luc and HT29-Luc cells were

522 purchased from the National Institute of Biomedical Innovation, Health, and Nutrition

523 (Osaka, Japan). RAS-less MEF cell lines (wild-type (wt) KRAS, KRAS G12D, KRAS

524 G12V, KRAS G12C, NRAS and HRAS) were obtained from the National Institutes of

525 Health (NCI RAS Initiative at the Frederick National Laboratory for Cancer Research,

526 Frederick, MD, USA).

527

528 **Animal studies.** BALB/cA-nu/nu and BALB/cA (female, 7-9 weeks old) were

529 purchased from CLEA Japan (Tokyo, Japan). The animals were maintained in

530 conventional housing conditions, with a daily 12-h light/dark cycle, and given food and

531 water *ad libitum*. The animals were cared for in accordance with the NIH Guide for the

532 Care and Use of Laboratory Animals. All animal experiments were approved by the

533 Committee on Animal Experimentation of the Tokyo University of Science.

534

535 **Reagents.** MLN2238 (A10600) was purchased from AdooQ BioScience (Irvine, CA,

536 USA). NAEi was purchased from AdipoGen (San Diego, CA, USA). Human 26S

537 Proteasome Protein (E-365) and Human 20S Proteasome Protein (E-360) were

538 purchased from R&D Systems (Minneapolis, MN, USA). Human KRAS (G12D) and

539 the corresponding His tag (12259-H07E1) were purchased from Sino Biological

540 (Beijing, China). Human KRAS (G12V), 2-186, and the corresponding His tag (R06-

541 32BH) were obtained from SignalChem Lifesciences (Richmond, British Columbia,

542 Canada).

543

544 **Measurement of 20S proteasome activity.** The chymotrypsin-like (β5), trypsin-like

545 (β2), and caspase-like (β1) activities of the 20S proteasome were measured using a 20S

546 Proteasome Activity Kit GOLD (StressMarq Bioscience Inc., Victoria, British

547 Columbia, Canada). Purified 20S proteasome (0.1 μg) was incubated in the presence of

548 CANDDY molecules (1, 4, 10, 20, 40, 80, and 160 μM) or MLN2238 at the indicated

549 concentrations for 30 min at room temperature. After incubation, 100 mM of

550 fluorogenic peptide substrates, Suc-LLVY-AMC (β5 substrate), Bz-VGR-AMC (β2

551 substrate), or Z-LLE-AMC (β1 substrate), was added, followed by incubation for 1 h at

552 room temperature. The reaction mixture was then transferred to a 96-well plate, and the

553 fluorecence from hydrolyzed AMC groups was measured using a Synergy HT multi-

554 channel microplate reader (BioTek Instruments, Inc., Winooski, VT, USA) with a 360

555 nm excitation filter and 460 nm emission filter.

556

557 **Evaluation of affinity of TUS-007 for KRAS in a thermal shift assay.** The KRAS

558 G12D/V (100 nM) was preincubated with TUS-007, a RAS-SOS inhibitor, or 10%

559 DMSO in 75 mM phosphate buffer (pH 7.5) for 30 min at 37 °C (G12D) or for 20 min

560 at 25 °C (G12V). Aliquots of the reaction solution were sampled into separate

561 microtubes and heated for 30 min at 70, 80, or 90 °C for G12D, or at 40, 50, or 60 °C

562 for G12V. After centrifugation at 18,000 ×*g* for 20 min, the supernatants were analyzed

563 by SDS-PAGE, followed by immunoblotting using an anti-KRAS antibody (1:1000,

564 WH0003845MI, Sigma-Aldrich, St. Louis, MO, USA). Immunoreactive bands were

565 detected using an iBright CL1000 chemiluminator (Thermo Fisher Scientific, Waltham,

566 MA, USA) with an enhanced chemiluminescent substrate for detection of horseradish

567 peroxidase (HRP; Merck, Darmstadt, Germany).

568

569 **Estiamtion of T_m values using fluorescence based thermal shift assay.** To estimate

570 the T_m values, we performed a fluorescence based thermal shift assay using ProteoStat

571 Thermal Shift Stability assay (ENZO Life Sciences, Farmingdale, NY, USA). 1 μg of

572 KRAS G12D was mixed with DMSO (2.5 %), RAS-SOS inhibitor (4 μM) or TUS-007

573 (4 μM) in 1x assay buffer containing a fluorescent indicator of protein destabilization,

574 ProteoStat TS Detection Reagent, and incubated under heating from 25 °C to 99 °C in

575 StepOne Plus Real-time PCR system (Thermo Fisher Scientific). The kinetics of

576 fluorescent signals were analyzed to calculate T_m values in Protein Thermal Shift

577 Software 1.3 (Thermo Fisher Scientific).

578

579 **Evaluation of KRAS degradation induced by TUS-007 in a cell-free system.** KRAS

580 G12D (final concentration: 5 ng/μL) and 26S proteasome (final concentration: 8 nM)

581 were incubated with TUS-007 (2, 3, 5, 10, 20, 40 μM), RAS-SOS inhibitor (40 μM),

582 RAS-SOS-NH_2 (40 μM) or DMSO in 20 mM Tris-HCl buffer (pH 7.5) containing 20%

583 glycerol for 3 h at 37 °C. To assess the effect of MLN on chemical knockdown, KRAS

584 G12D and 26S proteasome were incubated with DMSO or TUS-007 40 μM in the

585 presence or absence of MLN (1 μM) in the same condition. KRAS G12V (final

586 concentration: 5 ng/μL) and 26S proteasome (final concentration: 8 nM) were incubated

587 with TUS-007 at the indicated concentration or DMSO in 75 mM phosphate buffer,

588 containing 1% LABRASOL (Gattefossé, Saint-Priest, France), for 1 h at 37 °C. After

589 centrifugation at 14,000 ×*g* for 10 min, the supernatants were analyzed by SDS-PAGE,

590 followed by immunoblotting using an anti-KRAS antibody (1:1000, WH0003845MI for

591 G12D, Sigma-Aldrich; and 1:2000, F234 for G12V, Santa Cruz Biotechnology, Inc.,

592 Dallas, TX, USA). The immunoreactive bands were detected, as described above. The

593 DC_{50} values were calculated by a Rodbard approximation using the band intensity

594 obtained from four and three independent experiments for G12D. Immunoblotting was

595 performed as mentioned above.

596

597 **Cell proliferation assay.** To examine the effect of TUS-007 on cell proliferation, the

598 WST-8 assay (Cell Count Reagent SF; Nacalai Tesque, Kyoto, Japan) was performed.

599 RAS-less MEF cells, expressing human RAS, were plated in 96-well plates at a density

600 of 3×10^3 cells per well, cultured overnight, then treated with the indicated

601 concentrations of TUS-007 in 4% FBS containing medium (KRAS G12D), 10% FBS

602 containing medium (KRAS G12V) or serum-free medium (KRAS G12C, wt KRAS,

603 HRAS, NRAS) for 72 h. After incubation, cell viability was measured

604 spectrophotometrically using the WST-8 reagent. The culture medium was removed and

605 WST-8 reagent was mixed with the growth medium at a ratio of 1:10 (with a final

606 volume of 110 μL) and added to each well. The cells were incubated in an atmosphere

607 of 5% CO_2 at 37 °C for 1 to 2 h, and the absorbance at 450 nm was measured using the

608 aforementioned Synergy HT multi-channel microplate reader (BioTek Instruments,

609 Inc.).

610

611 **Evaluation of TUS-007 specificity in cells.** RAS-less MEFs were used to evaluate the

612 selective degradation by TUS-007. RAS-less MEFs expressing one of the human WT

613 RAS members (KRAS WT, HRAS WT, or NRAS WT) or KRAS G12C were plated

614 into 6-well plates at a density of 3×10^4 cells per well, cultured overnight, and treated

615 with the indicated concentrations of TUS-007 in serum-free medium for 72 h. RAS-less

616 MEFs expressing KRAS G12D or G12V were plated into 96-well plates at a density of

617 3×10^3 cells per well, cultured overnight, and treated with the indicated concentrations

618 of TUS-007 in 4% FBS or 10% FBS containing medium, respectively, for 72 h. The

619 cells were lysed using RIPA buffer (Nacalai Tesque., Kyoto, Japan). The lysates were

620 centrifuged at 18,000 ×*g* for 10 min. The supernatants were analyzed by western

621 blotting using mouse monoclonal antibodies specific to KRAS (1:1000,

622 WH0003845MI; Sigma-Aldrich) and glyceraldehyde 3-phosphate dehydrogenase

623 (GAPDH, 1:10000, sc-32233; Santa Cruz Biotechnology, Inc.) and rabbit polyclonal

624 antibodies specific for HRAS (1:1000, 18295-1-AP; Proteintech, Rosemont, IL, USA)

625 and NRAS (1:1000, 10724-1-AP, Proteintech). Immunoreactive bands were detected

626 using iBright CL1000 chemiluminator or LAS 3000 (Fujifilm, Tokyo, Japan) with an

627 enhanced chemiluminescent substrate for the detection of horseradish peroxidase (HRP;

628 Merck, Darmstadt, Germany). The intensity of the RAS band was quantified using

629 ImageJ software and normalized to the intensity of the GAPDH band.

630

631 **Measurement of KRAS protein levels in cells by western blotting.** SW620-Luc and

632 SW1990 cells were treated with 1% DMSO or TUS-007 in serum-free medium for 48 h

633 (SW620-Luc cells) or 72 h (SW1990 cells). The cells were lysed using a RIPA buffer

634 (Nacalai Tesque., Kyoto, Japan). The precipitates were separated from the soluble

635 fraction by centrifugation at 18,000 ×*g* for 20 min. The supernatants were analyzed by

636 western blotting with mouse monoclonal antibodies specific for KRAS (1:1000,

637 WH0003845MI; Sigma-Aldrich) and GAPDH (1:20000, sc-32233; Santa Cruz

638 Biotechnology, Inc.). The immunoreactive bands were detected by LAS-3000, as

639 described above. The intensity of the KRAS band was quantified using ImageJ software

640 and normalized to the intensity of the GAPDH band.

641

642 **Evaluation of caspase activity.** To measure caspase activity, SW1990 cells were plated

643 onto 96-well white plates and 96-well clear plates, at a concentration of 8×10^3

644 cells/well, in a medium containing 10% FBS. The plates were incubated overnight

645 without CO_2 equilibration at 37 °C. The medium was replaced with medium containing

646 2% FBS, DMSO, 100 μM TUS-007, 3 μM MLN2238, or 2.5 μM NAEi and incubated

647 for 96 h. SW620-Luc cells were plated onto 96-well white plates and 96-well clear

648 plates at 2×10^3 cells/well in medium containing 10% FBS. After overnight incubation,

649 the medium was replaced with FBS-free medium containing 1% L-glutamine, DMSO,

650 and 25, 100, or 500 μM TUS-007 for 48 h. The caspase 3/7 Glo assay (Promega,

651 Madison, WI, USA) was performed on the white plates according to the manufacturer's

652 protocol. The chemiluminescence intensity was measured with a Synergy HT plate

653 reader (BioTek). The cell viability was measured in the clear plates using the WST-8

654 assay, as described above. Caspase 3/7 activity was obtained as the chemical

655 luminescence intensity of the caspase 3/7 Glo assay normalized to the cell viability.

656

657 **Analysis of apoptosis by flow cytometry.** SW1990, SW620-Luc, and HT-29 cells

658 were seeded in 24-well plates, followed by the addition of compounds at the indicated

659 concentrations. After incubation for 48 h (SW620-Luc, HT-29) or 72 h (SW1990), the

660 cells were harvested using trypsin, washed with phosphate-buffered saline (PBS), and

661 pelleted by centrifugation at 110 $\times g$ for 5 min. The cells were resuspended in 85 μL of

662 binding buffer (Annexin V-FITC Kit, Medical & Biological Laboratories Co., Ltd.,

663 Nagoya, Japan). Subsequently, 10 μL of annexin V-FITC and 5 μL of propidium iodide

664 (PI) were added to each sample, followed by incubation in the dark at room temperature

665 for 15 min. After incubation, 400 μL of binding buffer was added to each sample on ice.

666 The cells were then analyzed using a FACSCanto II fluorescence-activated cell sorter

667 (BD Biosciences, Santa Clara, CA, USA) to detect the fluorescein isothiocyanate

668 (FITC) signal with excitation and emission filter wavelengths of 488 nm and 580 nm,

669 respectively, to detect the PI signal. Data were analyzed using FlowJo software

670 (FlowJo, Eugene, OR, USA).

671

672 **Subcutaneous xenograft model.** SW620-Luc (3×10^7 cells/mL) and SW1990 (5×10^7

673 cells/mL) cells were suspended in PBS, and 100 μL of the single-cell suspension was

674 transplanted subcutaneously into the right flanks of BALB/cA-nu/nu mice using a 26 G

675 syringe. Tumor volumes were calculated as the tumor length × width^2 × 0.5. When the

676 tumor volumes reached approximately 100 mm^3, the mice were randomized into

677 treatment and control groups of 6 to 8 animals per group. For i.p. treatment, TUS-007

678 was dissolved in DMSO and then diluted to a final concentration of 10% DMSO in 20%

679 polyethylene glycol (PEG) 400/Tween 80 (1:1 ratio). The TUS-007 solution was

680 administered intraperitoneally into the tumor-bearing mice at a dose of 80 mg/kg every

681 three days. The control mice were treated with the PEG/Tween vehicle alone. For p.o.

682 treatment, TUS-007 was suspended in 0.5% (w/v) carboxymethyl cellulose (CMC) and

683 administered p.o. at a dose of 80 mg/kg every three days. CMC (0.5% w/v) was

684 administered to control mice. Cetuximab was administered to an additional group of

685 SW620-Luc-implanted mice at a dose of 1 mg/mouse every three days.

686

687 **Orthotopic xenograft model.** The pGL4.51 (Luc2/CMV/Neo) vector (Promega) was

688 transfected into SW1990 cells. Successfully transfected cells were selected using G418.

689 SW1990-Luc cells were mixed with growth factor-reduced Matrigel (BD Biosciences)

690 on ice, at a ratio of 1:1 (v/v), to obtain a final cell density of 1.5×10^4 cells/μL. Ten

691 microliters of the cell suspension was injected directly into the pancreas of BALB/cA-

692 nu/nu mice using a 27 G syringe. Three days after cell transplantation, TUS-007

693 treatment was initiated in six mice. TUS-007 was suspended in 0.5% (w/v) CMC and

694 administered orally at a dose of 160 mg/kg every 3 days. CMC (0.5% w/v) was

695 administered to control mice (n = 6). Tumor luciferase activity was monitored based on

696 the bioluminescence intensity. Fifty microliters of D-luciferin (30 mg/mL in saline) was

697 injected subcutaneously in mice (Promega). Twenty minutes after the injection,

698 bioluminescence images were obtained using an IVIS Lumina LT (Perkin Elmer,

699 Waltham, MA, USA) with an exposure time of 15 s while the mice were under

700 isoflurane anesthesia (Wako, Tokyo, Japan).

701

702 **Measurement of RAS levels and downstream signaling molecule activation in**

703 **xenograft tumors.** KRAS expression in xenograft tumors and wt RAS protein

704 expression in pancreas were evaluated by immunohistochemistry and western blot

705 analysis. Tumor tissue and pancreas were harvested from the mice harboring

706 subcutaneous xenografts on day 21 of the TUS-007 administration. Tumor tissues were

707 harvested from the orthotopic xenograft mice on day 24 after the TUS-007

708 administration for consecutive 3 days starting on day 21. A portion of each sample was

709 fixed in 4% paraformaldehyde (Nacalai Tesque., Kyoto, Japan), embedded in paraffin,

710 then cut into 5 μm-thick sections. The sections were deparaffinized and incubated in

711 0.3% hydrogen peroxide in methanol for 30 min, and antigen retrieval was performed

712 using a 10 mM citrate buffer (pH 6.0) at 121 °C for 20 min. Tumor tissues were

713 subsequently blocked with 1% bovine serum albumin (BSA) in PBS for 30 min and

714 stained with primary antibodies specific for human KRAS (1:200, 12063-1-AP;

715 Proteintech), diluted in 1% BSA, followed by HRP-labeled secondary antibodies

716 (1:600, ab6721; Abcam, Cambridge, UK) in 1% BSA for 30 min at room temperature.

717 The sections were counterstained with hematoxylin and visualized with

718 diaminobenzidine (1.02924.0001; Merck). Digital images were obtained at 40×

719 magnification using a model BZ-9000 microscope (Keyence, Osaka, Japan). The area of

720 KRAS staining was quantified using ImageJ software, and the perimeter-to-area ratio

721 (KRAS-positive area/section) was calculated for a total of 30 images of 6 tumor

722 sections from each group. The remaining part of each tumor sample was homogenized

723 in a cell-lysis buffer (50 mM triethanolamine, 50 mM KCl, 5 mM $MgCl_2$, 0.25 M

724 sucrose, 1 mM phenylmethylsulfonyl fluoride, proteinase inhibitors (Nacalai Tesque.,

725 Kyoto, Japan), 1 mM dithiothreitol, and ribonuclease inhibitor (0.2 unit/μl, TaKaRa

726 Bio., Shiga, Japan) for western blot analysis, as described above. Mouse monoclonal

727 antibodies specific for KRAS (1:1000, WH0003845MI; Sigma-Aldrich), HRAS

728 (1:1000, 18295-1-AP; Proteintech, Rosemont, IL, USA), NRAS (1:1000, 10724-1-AP,

729 Proteintech) and GAPDH (1:20000, sc-32233; Santa Cruz Biotechnology, Inc.) and

730 rabbit antibodies specific for p-Erk1/2 (phospho-p44/42 MAPK) (1:1000, #4370; Cell

731 Signaling Technology, Beverly, MA, USA), Erk1/2 (p44/42 MAPK) (1:1000, #4695;

732 Cell Signaling Technology), p-Akt (1:2000, #4060; Cell Signaling Technology), and

733 Akt (1:2000; #4691; Cell Signaling Technology) were used for the

734 immunohistochemical staining. The immunoreactive bands were detected by LAS-3000

735 as described above. Quantitative analysis of the western blots was performed using

736 ImageJ software, and the results were normalized to the GAPDH band intensity.

737

738 **Measurement of apoptosis in xenograft tumors.** DNA fragmentation in the tumor

739 tissues was evaluated by a TdT-mediated dUTP nick-end labeling (TUNEL) assay.

740 Paraffin-embedded tissue sections (5 μm thick) were deparaffinized. The TUNEL

741 reaction was performed using the DeadEnd Fluorometric TUNEL System (Promega),

742 according to the manufacturer's instructions. Fluorescence images were acquired using a

743 BZ-9000 fluorescence microscope (Keyence). TUNEL-positive cells were identified

744 and counted using ImageJ software. In total, 30 images of 6 tumor sections were

745 analyzed from each group.

746

747 **Determination of TUS-007 in pancreas.** BALB/c mice were treated i.p. with TUS-007,

748 and pancreas tissue was collected at suitable time points. Approximately 30-60 mg of

749 tissue was homogenized in 0.6 mL of tissue-lysis buffer (50 mM Tris-HCl pH 8.0, 20

750 mM EDTA, 10 mM NaCl, 1% SDS) by Micro Smash MS-100 using stainless (5.5 ϕ) and

751 zirconia (1.0 ϕ) beads (TOMY SEIKO CO., LTD., Tokyo, Japan), and 1 μL propyl p-

752 hydroxybenzoate (4 mg/mL in DMSO) was added to each sample as an internal standard.

753 Lysates were centrifuged at 18,000 ×*g* for 10 min and 2.25 mL of methanol/chloroform

754 (ratio of 2:1) was added to the supernatants and the mixture was allowed to stand for 30

755 min at room temperature. Chloroform and distilled water (0.75 mL each) were added and

756 samples were centrifuged at 1,500 ×*g* for 15 min. The layer of chloroform was collected.

757 The supernatants were dried under reduced pressure and redissolved in the mobile phase.

758 TUS-007 was determined by HPLC (Alliance e2695, Waters Corporation., MA, USA)

759 using COSMOSIL® C18-AR-II column (150×4.6 mm, Nacalai Tesque., Kyoto, Japan) in

760 the isocratic elution mode with 0.1% trifluoroacetic acid (TFA) in 50:50 (v/v)
761 acetonitrile/water mobile phase at a flow rate of 1.0 mL/min. All reagents for the assay
762 were purchased from Nacalai Tesque. (Kyoto, Japan).
763
764 **Degradation of MDM2 in HCT-116 cells.** HCT-116 human colon-cancer cells were
765 treated with 1% DMSO or TUS-007 in serum-free medium for 24 h. The cells were
766 lysed using a RIPA buffer (Nacalai Tesque). The precipitates were separated from the
767 soluble fraction by centrifugation at 18,000 ×*g* for 20 min. The supernatants were
768 analyzed by western blotting using a rabbit polyclonal antibody specific for MDM2
769 (1:1000, sc-965, Santa Cruz Biotechnology, Inc.) and GAPDH (1:20000, sc-32233;
770 Santa Cruz Biotechnology, Inc.). The immunoreactive bands were detected by LAS-
771 3000, as described above. The intensity of the MDM2 band was quantified using
772 ImageJ software and normalized to the intensity of the GAPDH band.
773
774 **Statistical analyses.** Statistical significance was determined with JMP® Pro 14 (SAS
775 Institute Inc., Cary, NC, USA). An unpaired *t*-test was used to compare pairs of groups

776 under the assumption of normality. A one-way ANOVA with Dunnett's post hoc

777 analysis was used to compare sets of three or more groups. P-values < 0.05 were

778 considered statistically significant.

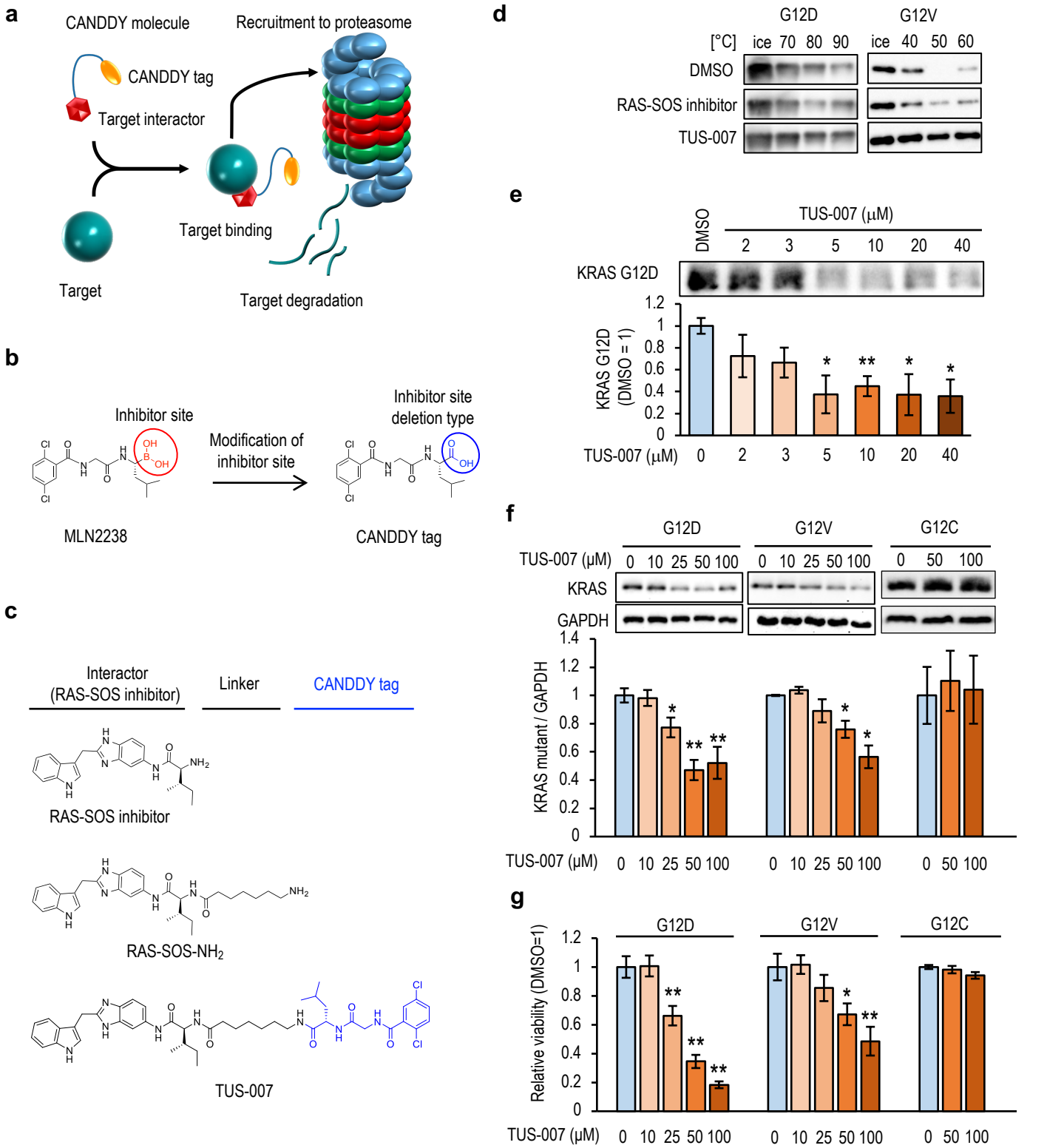

Fig. 1. RAS chemical knockdown *in vitro*.
a, Principle of the CANDDY technology. Each CANDDY molecule includes a target interactor (burgundy hexagon) and a CANDDY tag (yellow oval). The target protein is bound by the CANDDY molecule *via* the target interactor and is directly degraded by proteasome via the CANDDY tag. **b,** The CANDDY tag was synthesized by chemically inactivating the inhibitor site of MLM2238 (MLN). **c,** Structures of the RAS-SOS inhibitor (ref. 3), RAS-SOS-NH_2, and TUS-007. **d,** Evaluation of the target-binding affinity of TUS-007 to KRAS mutants by a thermal shift assay. Recombinant KRAS was treated with the vehicle, RAS-SOS inhibitor, or TUS-007 for 30 min, heated at the indicated temperature for 20 min, then analyzed by immunoblotting. **e,** KRAS G12D protein level was lower after incubation with TUS-007 at the indicated concentrations in the presence of 26S proteasome, indicating successful KRAS G12D degradation by TUS-007 (mean ± SEM; n = 3) . *P < 0.05 and ** P < 0.01 vs. DMSO. **f,** KRAS G12D and G12V levels, but not the G12C level, were decreased in RAS-less MEFs after incubation with TUS-007 for 72 h. Representative blots are shown. The relative amounts of KRAS mutants normalized to GAPDH are shown in the bar graph (mean ± SEM; n = 3–4). *P < 0.05 and ** P < 0.01 vs. DMSO. **g,** Decreased cell viability was observed in RAS-less MEFs expressing human KRAS G12D and G12V, but not those expressing G12C, after incubation with TUS-007 for 72 h (mean ± SEM; n = 3–4). *P < 0.05 and ** P < 0.01 vs. DMSO.

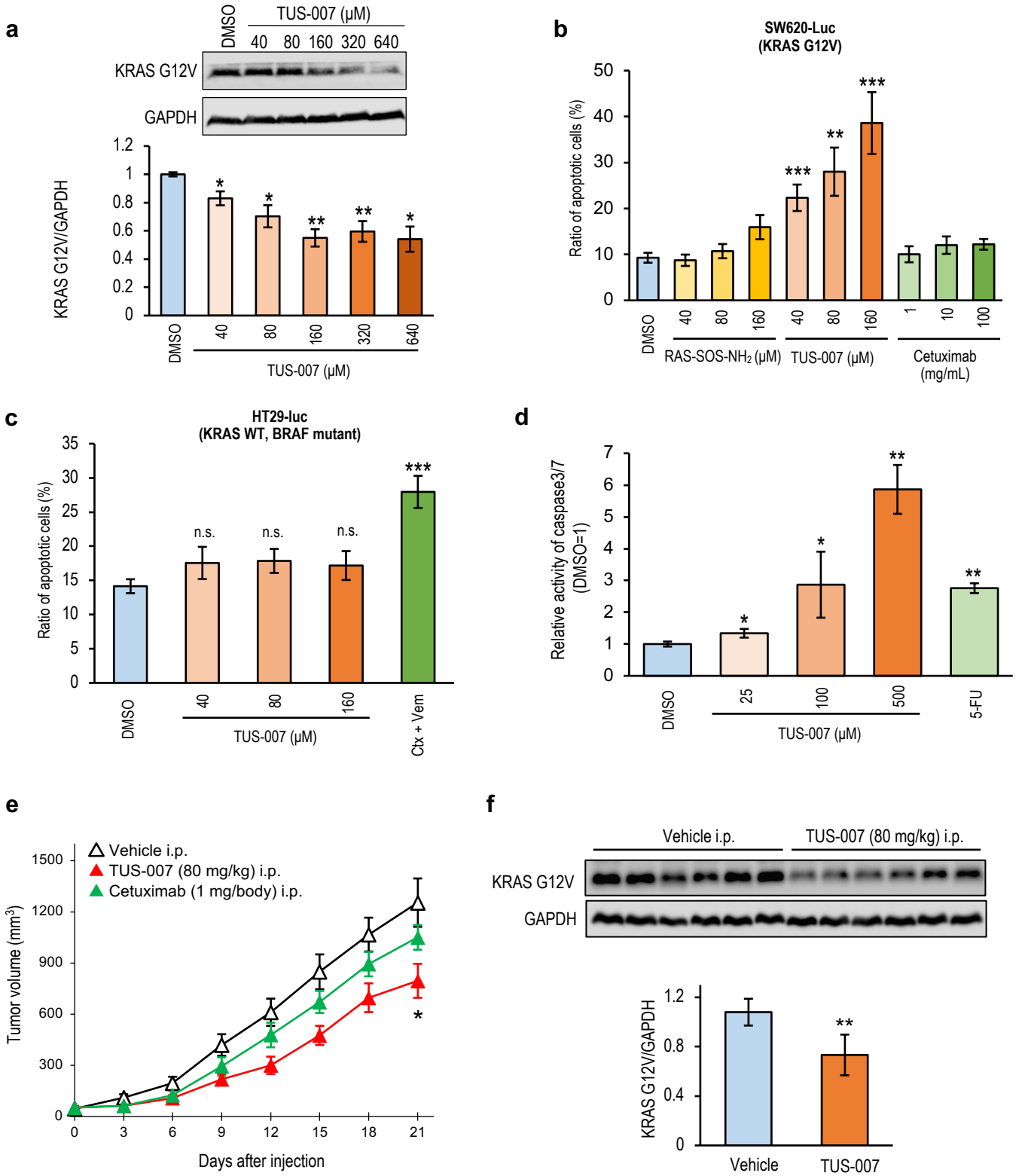

Fig. 2. Chemical knockdown and tumor suppression *in vitro* and *in vivo* in KRAS G12V-driven human colon cancer cells by TUS-007 treatment.

a, Immunoblotting analysis of KRAS G12V chemical knockdown in SW620-Luc cells treated with TUS-007 for 48 h at the indicated doses. The KRAS band intensity was normalized to that of GAPDH (mean ± SEM; n = 3). *P < 0.05 and ** P < 0.01 vs. DMSO. **b & c,** TUS-007 induced apoptosis in colon cancer SW620-Luc cells (**b**) but not in HT29-Luc cells (**c**), a KRAS-independent, BRAF-dependent cell line (Ctx + Vem: 100 μg/ml cetuximab and 40 μM vemurafenib). Cells were treated with each compound for 48 h in terms of the number of annexin V-positive/PI-negative apoptotic cells detected by flow cytometry (mean ± SEM; n = 2–5). **P < 0.01, and ***P < 0.001 vs. DMSO. **d,** Relative activity of caspase 3/7 in SW620-Luc cells treated with TUS-007 or 5-fluorouracil (5-FU) for 48 h (mean ± SEM; n = 3). *P < 0.05 and ** P < 0.01 vs. DMSO. **e,** Tumor volume in mice with SW620-Luc cells transplanted subcutaneously and treated with i.p. administration every 3 days (mean ± SEM; n = 6–8). *P < 0.05 vs. vehicle alone. **f,** Immunoblotting of KRAS G12V chemical knockdown in tumors from the same mice used in **e** (mean ± SEM; n = 6). **P < 0.01 vs. vehicle alone.

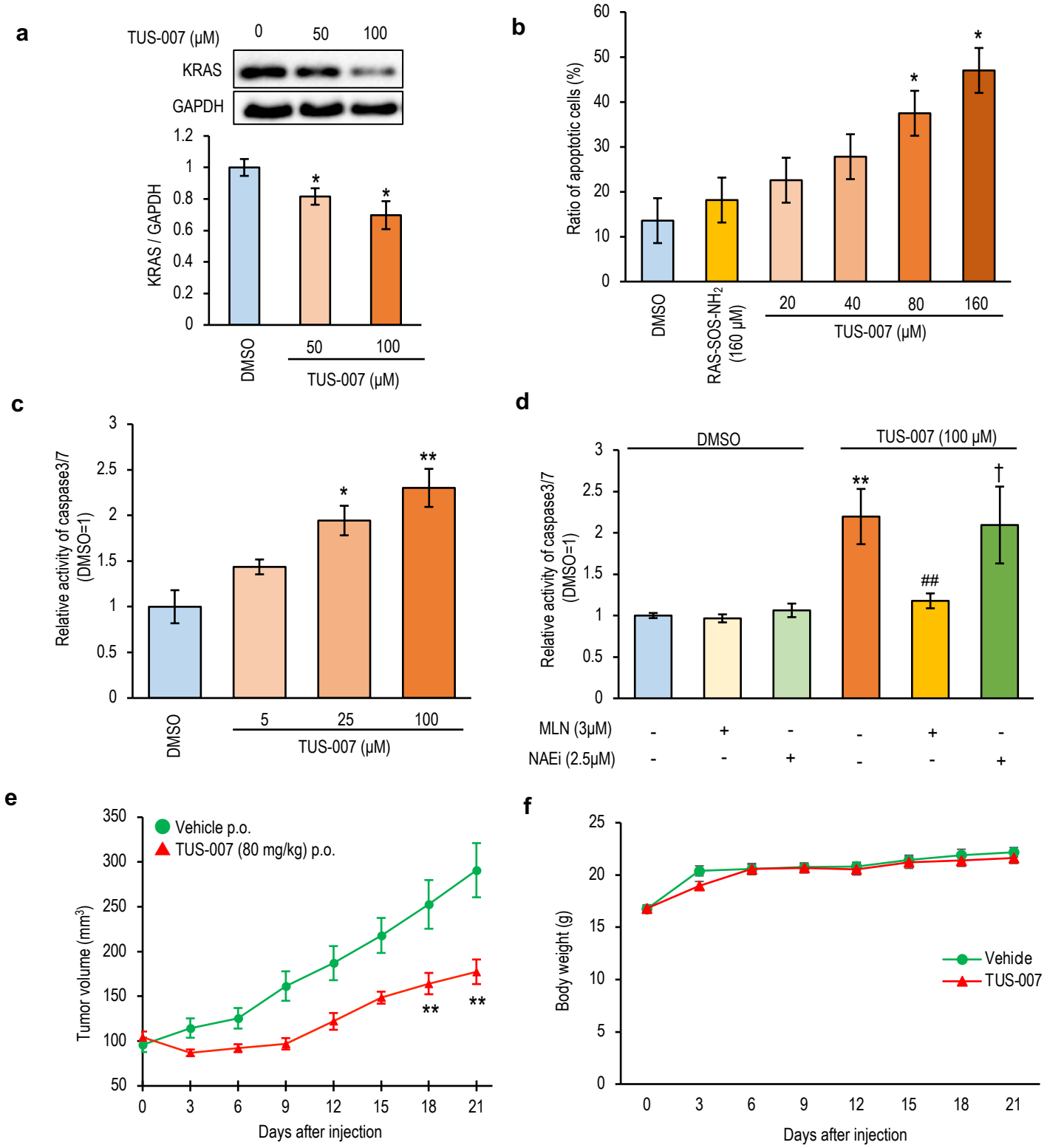

Fig. 3. Chemical-knockdown and tumor suppression *in vitro* and *in vivo* in KRAS G12D-driven human pancreatic cancer cells by TUS-007 treatment.

a, KRAS G12D chemical knockdown induced by TUS-007 in SW1990 cells. SW1990 cells were treated with TUS-007 for 72 h and analyzed by immunoblotting. The KRAS G12D band intensity was normalized to that of GAPDH (mean ± SEM; n = 4). *P < 0.05 vs. DMSO. **b,** TUS-007 treatment for 72 h increased the proportion of annexin V-positive apoptotic SW1990 cells compared with those treated with DMSO or RAS-SOS-NH_2 (mean ± SEM; n = 3). *P < 0.05 vs. DMSO or RAS-SOS-NH_2. **c,** TUS-007 increased the caspase 3/7 activity in SW1990 cells after treatment for 96 h (mean ± SEM; n = 3). *P < 0.05 and **P < 0.01 vs. DMSO. **d,** Caspase 3/7 activation by TUS-007 was counteracted by proteasome inhibition by MLN2238 (MLN) but not by E3 ligase inhibition by NAE inhibitor in SW1990 cells treated with the agents for 96 h (mean ± SEM; n = 3). **P < 0.01 vs. DMSO, ##P < 0.01 vs. TUS-007 (100 μM) only, and †no statistically significant difference compared with TUS-007 (100 μM) only. **e,** Tumor volume in mice with SW1990 cells transplanted subcutaneously and treated with p.o. administered TUS-007 or vehicle (mean ± SEM; n = 6–9). The agents were administered every 3 days. **P < 0.01 vs. vehicle alone. **f,** Body weight changes in mice with SW1990 cells transplanted subcutaneously (mean ± SEM; n = 6–9). P.o. treatment with TUS-007 did not affect the body weight.

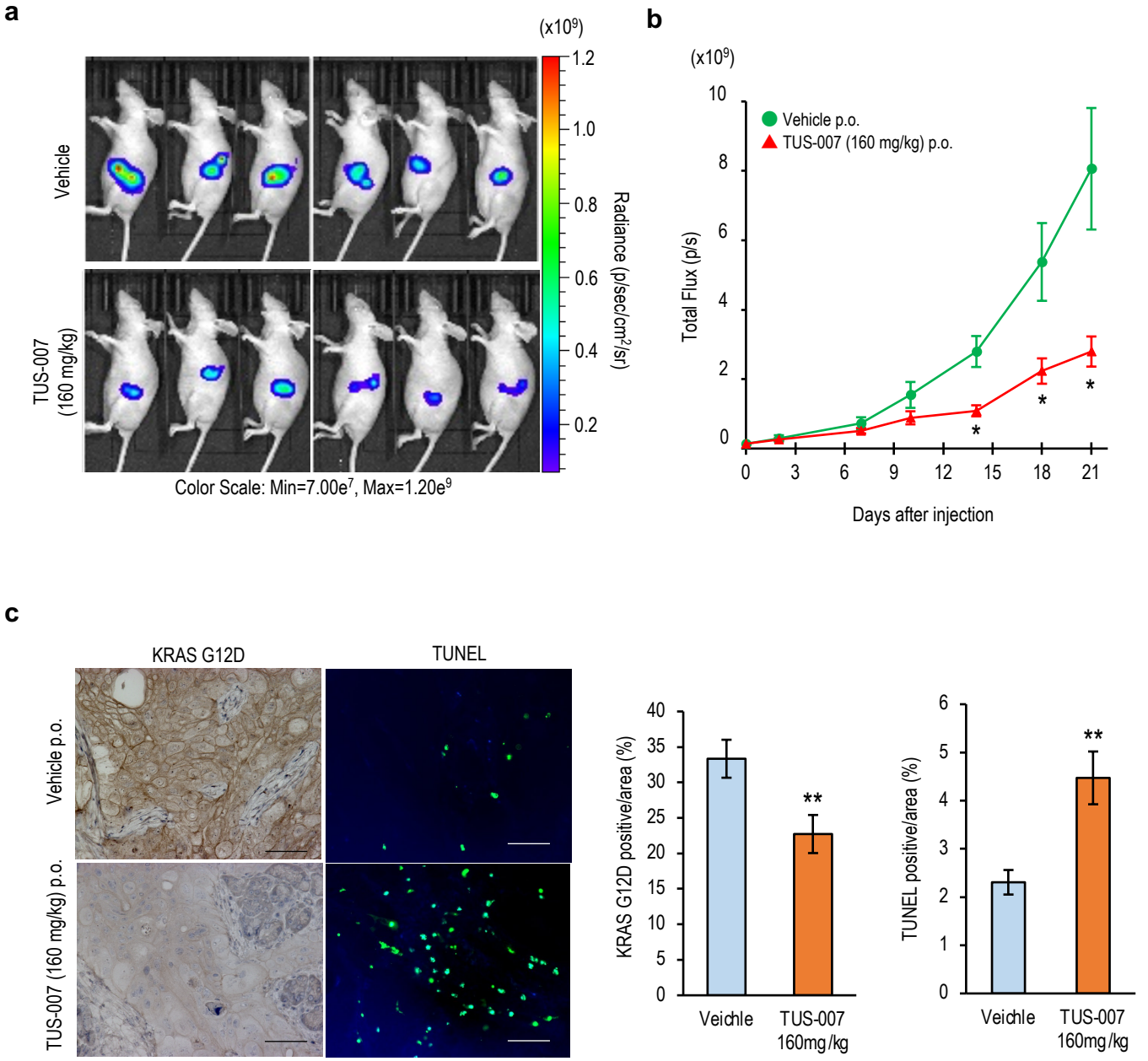

Fig. 4. TUS-007 suppresses the growth of KRAS G12D-positive orthotopic pancreatic tumors.
a, Images showing the luciferase activity and total flux in orthotopic tumors transplanted SW1990-Luc cells *in vivo*. **b,** Tumor growth (bioluminescence) in identical mice treated with vehicle or TUS-007 administered p.o. every 3 days. (mean ± SEM; n = 6). *P < 0.05 vs. vehicle alone. **c,** Representative histochemical staining of KRAS and TUNEL in orthotopic tumor sections from the same mice used in **a**. The scale bar is 60 μm. The bar graphs showed quantitative analyses of the KRAS G12D-positive area (left) and TUNEL-positive area (right) (mean ± SEM; n = 6). **P < 0.01 vs. vehicle alone.